

Interpretable similarity-driven multi-view embeddings from high-dimensional biomedical data

Brian B. Avants, PhD, Nicholas J. Tustison, DSc, James R. Stone, MD, PhD, and the Pediatric Imaging, Neurocognition, and Genetics Study*

Department of Radiology and Medical Imaging, University of Virginia, Charlottesville, VA

Corresponding author:
Brian B. Avants, PhD
Department of Radiology and Medical Imaging
University of Virginia
480 Ray C Hunt Drive
Box 801339
Charlottesville, VA 22903
434-924-9585
stnava@gmail.com

*Data used in preparation of this article were obtained from the Pediatric Imaging, Neurocognition and Genetics Study (PING) database (<http://ping.chd.ucsd.edu>). As such, the investigators within PING contributed to the design and implementation of PING and/or provided data but did not participate in analysis or writing of this report. A complete listing of PING investigators can be found at <https://ping-dataportal.ucsd.edu/sharing/Authors10222012.pdf>

Abstract

Similarity-driven multi-view linear reconstruction (SiMLR) is an algorithm that exploits inter-modality relationships to transform large scientific datasets into smaller, more well-powered and interpretable low-dimensional spaces. SiMLR contributes a novel objective function for identifying joint signal, regularization based on sparse matrices representing prior within-modality relationships and an implementation that permits application to joint reduction of large data matrices, each of which may have millions of entries. We demonstrate that SiMLR outperforms closely related methods on supervised learning problems in simulation data, a multi-omics cancer survival prediction dataset and multiple modality neuroimaging datasets. Taken together, this collection of results shows that SiMLR may be applied with default parameters to joint signal estimation from disparate modalities and may yield practically useful results in a variety of application domains.

Keywords: code:R, multi-modality embedding, brain, ANTs, ANTsR, genotype, depression, SiMLR, imaging genetics

1 Introduction

Healthcare – from both a prevention as well as treatment perspective – is increasingly turning to large, mixed datasets to gain a better understanding of the biological complexity that influences sensitivity or resistance to disease, injury, etc. In the case of rare diseases, multi-view datasets are collected to build a more complete characterization of disease phenotype and potentially gain insights into etiology. In more common conditions, like Alzheimer’s disease, multi-view datasets are motivated by the need to understand the diversity of the disease process, identify sub-groups and thereby advance personalized treatment approaches. Multi-view data can also provide insight into the features that drive variability within the “normal” phenotype e.g. underlying factors that contribute to difference in neurobiological age¹ or the genetic architecture of quantitative phenotypes as mediated through brain structure².

Multi-view (also known as multiple modality or multi-block) datasets are increasingly common in the biomedical sciences. In the idealized case, each view / modality will provide a completely unique measurement of the substrate biology. However, it is perhaps more common that each view provides a partial and not wholly independent perspective on a complex phenomenon. In this case, covariation can be exploited in order to sift through noisy measurements and better identify meaningful signal. Moreover, joint relationships across systems of the brain or across scale can form the foundation for integrative scientific hypotheses.

Pre-specified joint hypotheses allow the scientist to avoid a combinatorial explosion of tests for possible interactions. Although powerful in sufficiently large, well-understood datasets, prior multivariate hypotheses can be difficult to enumerate with sufficient detail to support implementation and testing. Fully multivariate and data-driven dimensionality reduction models provide an alternative including principal component analysis (PCA)^{3,4} and independent component analysis (ICA)⁵⁻⁷. However, these popular models, applied directly, are not explicitly designed for interpretation across multiple modalities and do not provide an easy way for the scientist to regularize the solution with prior knowledge or to visualize the feature vectors which are both dense and signed (i.e. have both positive and negative weights).

Graph-regularized, imaging-focused dimensionality reduction methods emerged in recent years to address the desire for interpretable components⁸⁻¹⁰. **Graph-net**¹⁰, similar to **SCCAN**^{11,12}, uses ℓ_1 regularization to constrain embedding vectors to be sparse and reduce over-fitting in high-dimensional problems. Relatedly, graph-regularization has been used to improve prediction in imaging genetics^{10,13,14} and may be combined with canonical correlation analysis (as in **SCCAN**¹¹). Non-negative factorization methods provide a second degree of interpretability by guaranteeing that factorizations are unsigned and, therefore, allow components to be interpreted in terms of their original units (e.g. millimeters)^{15,16}. Other efforts^{9,17} use prior constraints to guide solutions toward familiar sparsity patterns. More generally, regularization is also critical to well-posedness^{18,19}.

The need for joint, interpretable modeling of several (>2) parallel but heterogenous datatypes is rapidly increasing²⁰⁻²⁴. Multi-block data analysis methods such as Kettering’s five offerings²⁵ and more recent regularized generalized canonical correlation analysis (RGCCA and its sparse variant SGCCA)²⁶⁻²⁸ and multiway generalized canonical correlation analysis²⁹ extend

Hotelling’s classical CCA^{30,31} to multi-view (viz. multi-block) data. Joint and individual variation explained (JIVE) is another framework dedicated to data fusion^{32,33} along with MultiLevel Simultaneous Component Analysis (MLSCA)³⁴ and Multi-Omics Factor Analysis (MOFA)³⁵. A variation of JIVE, applied to convolutional network features, has also been applied to imaging genetics problems³⁶.

Our contribution, similarity-driven multi-view linear reconstruction (SiMLR), is a new joint embedding method—targeting biomedical data—that links several of the ideas expressed in prior work. SiMLR builds on sparse canonical correlation analysis for neuroimaging (SCCAN)^{12,37,38} and prior-based eigenanatomy^{17,39}. SiMLR goes beyond SCCAN in that it takes two or more modalities as input, allows customized regularization models and uses a fast and memory efficient implementation appropriate for large datasets. SiMLR outputs locally optimal low-dimensional matrix embeddings for each modality that best predict its partner modalities. SiMLR achieves this by reconstructing each modality matrix from a basis set derived from the partner modalities. One novel aspect of SiMLR is that the “linking” basis set is computed via a source separation algorithm, e.g. singular value decomposition (SVD) or ICA. This sub-algorithm seeks to identify latent signal sources that span modalities. The basis set can be forced to be either orthogonal (SVD) or statistically independent (ICA) where the latter option may be more appropriate for unmixing signal sources in real world data^{40,41}. Simultaneously, the feature vectors may be constrained by graph-regularized sparsity and non-negativity. Furthermore, the target energy (measuring the similarity between different modalities) is also flexible and builds on classical objective functions in SVD and CCA. SiMLR is the only available framework that combines these features in an accessible and flexible joint dimensionality reduction algorithm. ¹

2 Results

Figure 1 shows a general overview of how SiMLR is applied within the context of scientific data. Each evaluation below fits within this general framework. Furthermore, each study uses joint dimensionality reduction in conjunction with regression-based supervised learning in a training and testing paradigm. Table 1 summarizes the overall findings that are presented in this results section and demonstrates a ranking of performance based on the included evaluation metrics. The results below are all drawn from the following location where the underlying reproducible computational practices are made available to readers: <https://codeocean.com/capsule/9877797/>. From here, this location will be referred to simply as `codeocean` and specific files therein will be referenced by filename as they appear in the `results` section of the capsule.

2.1 Terminology

We outline the terminology used in the discussion that follows.

¹Although SiMLR supports path modeling, only the leave-one-modality-out approach is explored in this work.

- **Multi-view:** several modalities collected in one cohort; alternatively, the same measurements taken across different studies⁴². We focus on the first case here.
- **Covariation:** we use the term in two contexts. As a general concept, we mean systematic changes in one modality are reflected in a predictable amount of change in other modalities. In the mathematical context, we use the definition of covariation for discrete random variables.
- **Latent space/embeddings:** both terms refer to an (often lower-dimensional) representation of high-dimensional data. These are also known as components in PCA. In the context of this paper, we are approximating the (hidden) latent space with the learned embeddings. Often, the true latent space cannot be known. We compute embeddings (or components), here, by multiplying feature vectors against input data matrices. Importantly, SiMLR can compute latent spaces that target either statistical independence (the ICA source separation algorithm⁴⁰) or orthogonality (the SVD algorithm). Deflation-based schemes, on the other hand, only target orthogonality.
- **Feature vectors:** these are weights on the original features. In SiMLR, the feature vectors are the solutions that we are seeking. Projecting the feature vectors onto the original data will provide a low-dimensional representation.

These concepts are expanded upon in more detail in the methodology section.

2.2 Data representation

SiMLR assumes “clean” data as input. This data has no missing values and is structured in matrix format with each modality matched along rows (here, these are the subjects/samples). Single nucleotide polymorphism (SNP) data is often formatted this way after imputing to a common reference dataset such as the HapMap. In neuroimaging, we employ region of interest measurements or spatial normalization in order to map a high-dimensional image into this common representation. For example, if a brain template has p voxels within the cortex and the population contains n subjects, then the matrix representation of the population level voxel-wise, normalized cortical thickness map will be $X_{\text{thickness}}$ with dimensions $n \times p$. SiMLR accepts > 1 matrices organized in this manner. A study of m distinct modalities would have input matrices with dimensions $n \times p_i$ (subjects \times predictors), noting that p_i need not equal p_j for any $i, j \in 1, \dots, m$.

2.3 Simulation data and comparison to RGCCA, SGCCA

SiMLR seeks to solve a multiple modality version of the cocktail party problem⁴³ where the hidden source signals are distributed across each modality. Therefore, SiMLR assumes that this common latent signal exists across modalities and may be found by linear projections into a low-dimensional space. We construct simulated data that matches this setting by constructing 3 matrices from different (modality-specific) multivariate distributions. Each matrix contains a common low-dimensional basis (the true latent signal), as illustrated in Figure 2, which can be recovered by joint dimensionality reduction. Matrices are generated by the following steps.

- Generate a rank- K basis set (S_j^K of size $K \times p_j$ where $j \in 1, 2, 3$) of gaussian distributed signal that is smoothed by a different amount over each simulation run; K and p_j vary over simulations.
- Generate ground truth latent signal matrix $B = [\vec{\beta}_1, \dots, \vec{\beta}_K]$ with n rows that will weight each basis matrix S_j^K . B is consistent across all modalities but n varies across simulations.
- Generate each $n \times p_j$ data matrix by computing $M_j = B S_j^K$.
- Replace a percentage of the columns of each matrix M_j with random noise.
- Split the data into 80% train and 20% test and run the candidate algorithms on each M_j^{train} matrix. Lastly, use linear regression to relate the learned embeddings to the true source signal ($\vec{\beta}_1^{\text{train}}$) and predict $\vec{\beta}_1^{\text{test}}$ in the test data from the learned embeddings.

The above steps produce data where each of the three 3 matrices is generated from very different distributions but that contain a common latent signal. The key is that the latent signal is at least partially consistent ($\vec{\beta}_1$) and can, in some cases, be recovered by joint analysis. Recoverability varies across simulations due to both corruption and the intrinsic variability of the underlying generating distributions.

The evaluation criterion then compares the ability of SiMLR to recapture the known basis with respect to: (a) regularized generalized canonical correlation analysis (RGCCA); (b) sparse generalized canonical correlation analysis (SGCCA); (c) permutations of the original data. The primary evaluation criterion – accuracy in predicting the true latent signal – exhibits that SiMLR’s use of cross-modality information and regularization drives the solution closer to the ground truth basis in comparison to the other methods. Secondly, we demonstrate improved robustness to data corruption. The permutation comparison contrasts the SiMLR solution to that which would be found when no covariation across modalities exists.

2.3.1 Signal recovery

An overview of the results is in Figure 3. For each experiment, we run 120 simulations and evaluate the quality of the recovered signal by training a linear regression algorithm to relate the learned basis to the true basis. We then predict the latent signal in held-out test data (80 percent of subjects are used for training and 20 percent for testing). In this scenario, better performing methods will lead to more accurate predictions of the latent signal in the

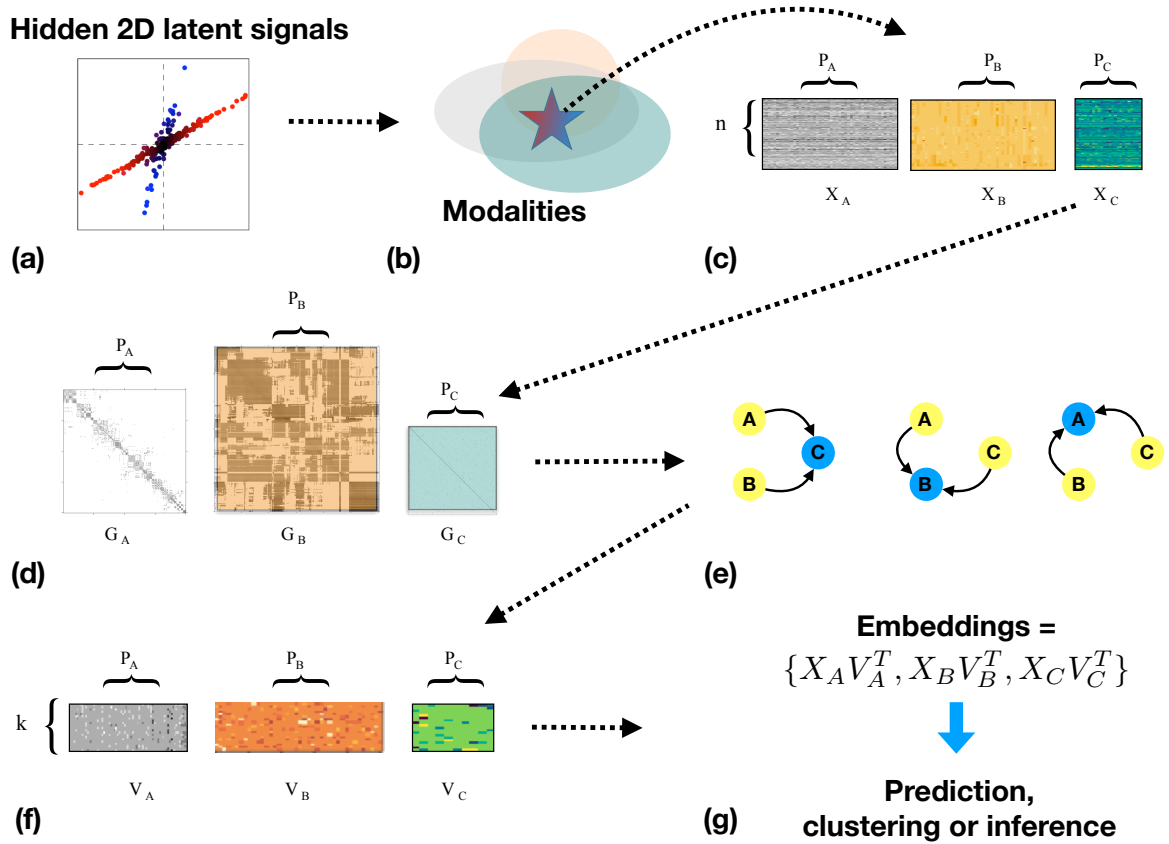


Figure 1: Example SiMLR study overview: (a) Two statistically independent signals are shown here to represent the hidden latent signal potentially two components of a disease process; (b) This latent signal is distributed across different subjects each of whom is measured with multi-omics. (c) The data is converted to matrices; in this effort we focus on matrices with common number of subject here denoted by n and variable number of predictors ($p_{A,B,C}$). (d) Sparse regularization matrices (G) are constructed with user input of domain knowledge or via helper functions; (e) SiMLR iteratively optimizes the ability of the modalities to predict each other in leave one out fashion; (f) Sparse feature vectors emerge which can be interpreted as weighted averages over select columns of the input matrices that maintain the original units of the data. These are used to compute embeddings in (g) and passed to downstream analyses. Alternatively, one could permute the SiMLR solution to gain empirical statistics on its solutions.

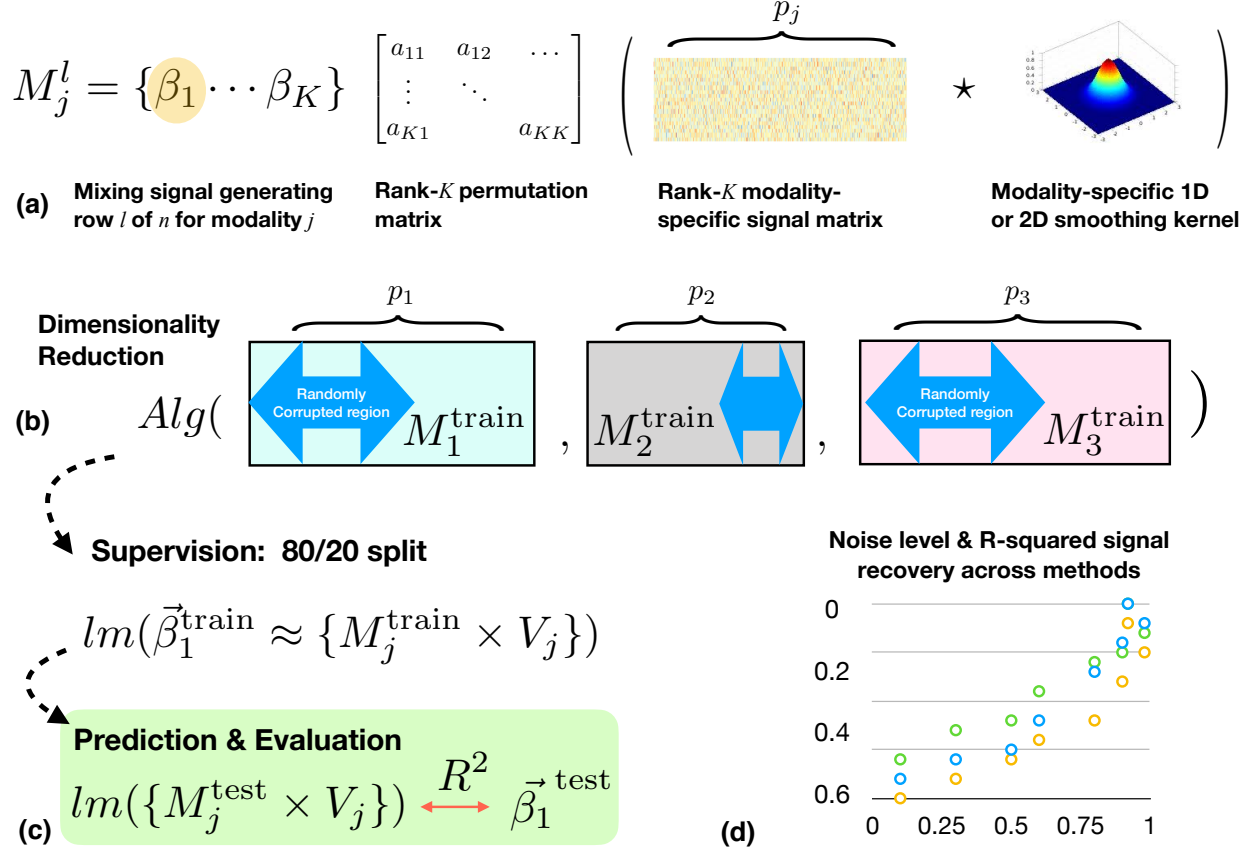


Figure 2: Conceptual overview of the SiMLR simulation study which defines an inverse problem for signal recovery with known ground truth. (a) shows the generation of a given row, M_j^l , in a single simulated matrix, M_j . The K -rank generating basis set is smoothed to induce signal-specific covariation as is present in many types of real biological data. The highlighted beta is the common signal that we seek to recover. (b) The study also randomly corrupts each of the three generated matrices by eliminating any true signal in some fraction of the matrix. The fraction of corruption is drawn from a uniform distribution between 0.1 and 0.9 (i.e. 10 and 90 percent corruption). (c) We define a random 80/20 split for each simulation and learn from the 80 percent of training data. RGCCA, SGCCA and SiMLR are each run in the dimensionality reduction step. A linear regression method takes the low-dimensional embeddings, the ground truth signal in the training data and then predicts the test data signal. (d) This process enables us to evaluate the signal recovery performance and how it is impacted by the corruption process.

testing subjects. We can evaluate, by paired t -test on the recovery (measured by R^2 of the fit), whether SiMLR performs better than, equal to or worse than other methods.

The experiments are available in the `codeocean` capsule via source `simulationStudyRGCCA.Rmd` and with recovery outputs detailed below for each experiment:

- [simulationStudyRGCCA_CCA_mix_ICA.html](#): The CCA-like objective function with ICA for source separation (SiMLR-CCA-ICA). Mean signal recovery R^2 is 0.5043659 with paired t -test relative to RGCCA showing relative improvement at $t = 13.27$, p -value $< 2.2e - 16$ and paired t -test relative to SGCCA showing $t = 5.0594$, p -value $= 1.546e - 06$.
- [simulationStudyRGCCA_CCA_mix_SVD.html](#): The CCA-like objective function with SVD for source separation (SiMLR-CCA-SVD). Mean signal recovery R^2 is 0.51233675 with paired t -test relative to RGCCA showing relative improvement at 12.746, p -value $< 2.2e - 16$ and paired t -test relative to SGCCA showing $t = 5.4298$, p -value $= 3.028e - 07$.
- [simulationStudyRGCCA_Reg_mix_ICA.html](#): The regression (reconstruction) objective function with ICA (SiMLR-Reg-ICA). Mean signal recovery R^2 is 0.49118147 with paired t -test relative to RGCCA showing relative improvement at $t = 12.008$, p -value $< 2.2e - 16$ and paired t -test relative to SGCCA showing $t = 3.5184$, p -value $= 0.0006158$.
- [simulationStudyRGCCA_Reg_mix_SVD.html](#): The regression (reconstruction) objective function with SVD (SiMLR-Reg-SVD). Mean signal recovery R^2 is 0.49395552 with paired t -test relative to RGCCA showing relative improvement at $t = 11.99$, p -value $< 2.2e - 16$ and paired t -test relative to SGCCA showing $t = 3.7482$, p -value $= 0.0002763$.

The best overall was SiMLR-CCA-SVD with an average R^2 recovery of 0.51 while SGCCA and RGCCA score 0.45 and 0.35 respectively.

2.3.2 Sensitivity to amount of corrupted data

As above, for each of the 120 simulations, a varying degree of corruption to each matrix is performed. That is, a random percentage of the matrix that contains true signal is replaced with noise signal with no relationship to the latent ground truth. The amount of corruption varies between 10 and 90 percent of the column entries. This enables us to test the degree to which recovery performance can be predicted from the amount of corruption where corruption is represented as a 3-vector for each experiment where each entry in the vector codifies the amount of corruption. RGCCA performance (R^2) is related to corruption with p -value 0.01179. SGCCA performance is related with p -value 0.0001525. SiMLR-CCA-ICA is related with p -value 0.01045. SiMLR-CCA-SVD is related with p -value 0.04103. SiMLR-Reg-ICA is related with p -value 0.0223. SiMLR-Reg-SVD is related with p -value 0.006516. As such, SGCCA (in this experiment) is most sensitive of these methods to corrupted data and SiMLR-CCA-SVD is least so. Inspection of the R^2 performance plots indicates that the impact of corruption is not insubstantial with 24 of 120 RGCCA experiments leading to

R^2 less than 0.2. For SGCCA, SiMLR-CCA-ICA, SiMLR-CCA-SVD, SiMLR-Reg-ICA and SiMLR-Reg-SVD, these totals are 13, 6, 5, 3 and 4 respectively. From this perspective of a performance cutoff, SGCCA does slightly better than RGCCA. However, both methods still are less reliable than all variants of SiMLR. In the remaining evaluation studies, we focus on contrasting SGCCA with SiMLR because they both involve feature selection which is more appropriate for the $p \gg n$ cases that we investigate.

2.3.3 Recovery of two latent signals

A novel hallmark of SiMLR's design is that it relies on source separation to define the intermediate latent space used during the optimization of its feature matrices. This suggests that SiMLR should exhibit improved recovery of not just a single latent vector space (as above) but several at once. We demonstrate this advantage in an experiment that follows the same design as above but evaluates recovery of two latent signals. As expected, SiMLR outperforms SGCCA to an even greater degree in this more challenging scenario where, for the second signal to be recovered, SiMLR outperforms SGCCA as measured by paired t -test (239 degrees of freedom, $t = 6.41$, t -value = $7.55e-10$). The details of these results are in supplementary information and the experimental code is here (link): http://github.com/stnava/symmlrExamples/blob/master/figures/simulationStudyRGCCA_2components.pdf.

2.4 Cancer survival prediction from multi-omic data

We compare dimensionality reduction methods with respect to glioblastoma (GBM) survival prediction based on multi-omics data. The biological data includes $n = 208$ subjects with:

- Gene expression: with $p = 20,531$ predictors; see⁴⁴ for more information on this modality;
- Methyloomics/DNA methylation: with $p = 5,000$ predictors; see⁴⁵ for background;
- Transcriptomics/micro RNA expression: with $p = 1,046$ predictors; see⁴⁶ for background;

and is complemented by survival data (number of days since diagnosis and whether or not death has occurred at that time). Additional cohort information, such as age and gender, is also available but was not used here ²

The hypothesis is that this collection of measurements, which track the biological/genetic dynamics of tumor activity, will improve prediction of patient-specific outcomes. However, these data are fairly high-dimensional relative to the number of subjects. As such, targeted dimensionality reduction is needed to overcome the $p \gg n$ problem (where p , here, refers to predictors) in order to allow low-dimensional versions of these predictors (i.e. embeddings) to be used in a classical regression context.

The model is a Cox proportional hazards regression model⁴⁷ implemented in the `coxph` function in the `survival` package⁴⁸. We evaluate concordance in test data via the `survcomp` package. Concordance is similar to a rank correlation method and is used to assess agreement of the predicted outcomes (chance of death, given survival time and the multi-omic predictors) with true outcomes. Its value under the null hypothesis of no predictive value is 0.5. Values greater than roughly 0.6 show some evidence of predictive power in this application context^{49,50}. Data is the GBM set from [the multi-omic benchmark collection](#). The published paper associated with this benchmark is⁵¹. We chose the GBM data as it allowed a train-test split with sufficient variability of survival with respect to the n in both train and test groups, in particular in the latter. GBM shows among the highest differential survival among clusters reported in⁵¹. These data are collected from The Cancer Genome Atlas (TCGA).

The benchmark paper above showed that “with respect to survival, MCCA had the total best prognostic value” where MCCA refers to multiple canonical correlation analysis (pairwise CCA across all pairs)⁵². Thus, the comparison between SGCCA and SiMLR is pertinent. Nevertheless, these approaches should not be considered as the best strategy given that single-omic analysis did nearly as well. The authors find that “analysis of multi-omics data does not consistently provide better prognostic value and clinical significance compared to analysis of single-omic data alone, especially when different single-omics are used for each cancer types”.

The study design is fairly simple. For both SGCCA and SiMLR and over 50 runs, we:

²We have results from experiments that include more demographic data along with multiomics to predict survival in not only GBM but also KIRC and melanoma. This may be shared publicly in the future after more validation of the data organization. Please contact the authors if interested.

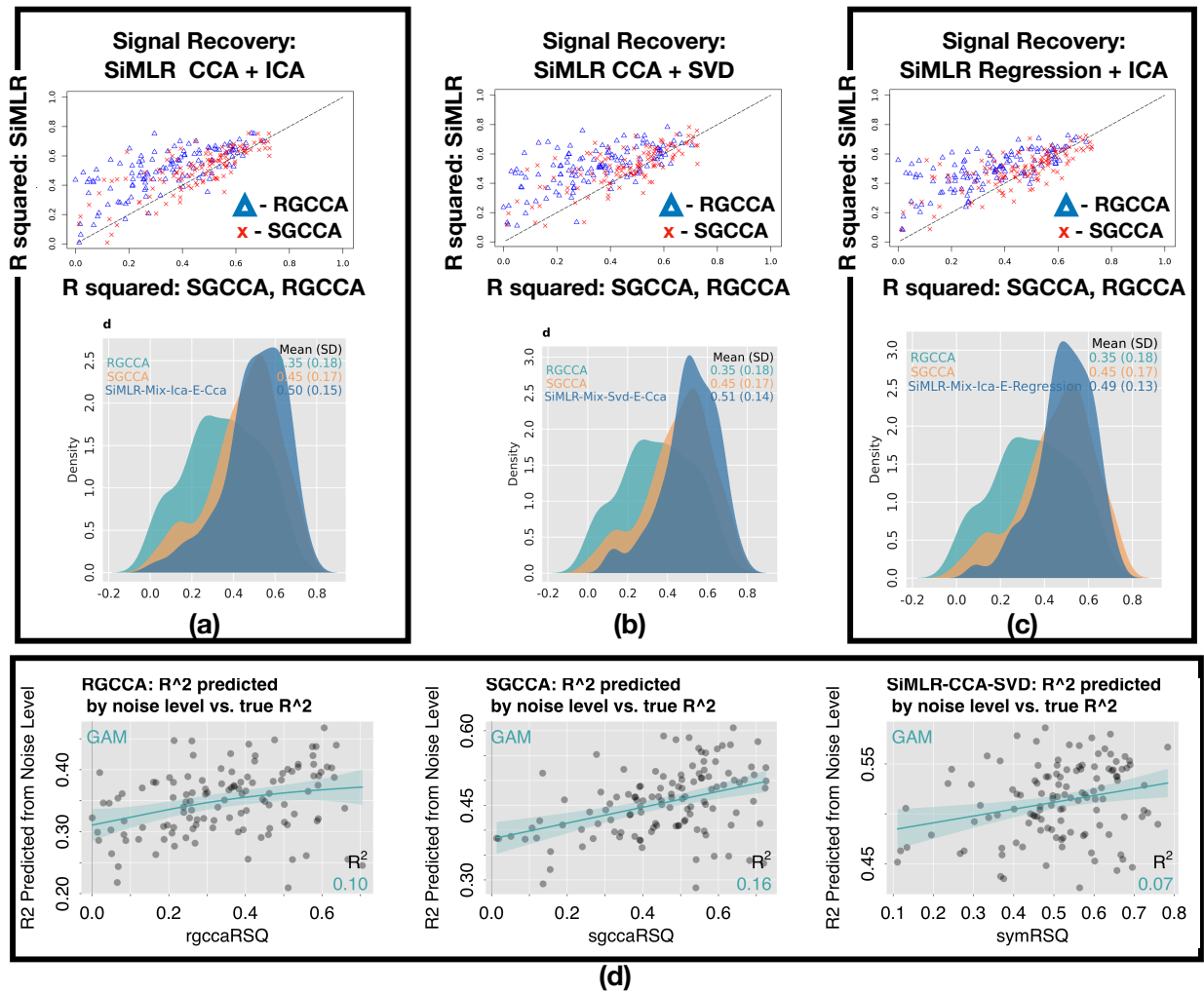


Figure 3: SiMLR simulation study results: sensitivity to noise and ability to recover signal. In each panel, (a-c), the SiMLR signal recovery performance in terms of R^2 is plotted against RGCCA and SGCCA performance. Thus, higher scores are better and points above the diagonal dotted line show superior SiMLR performance in pair-wise fashion. (a) Demonstrates performance of signal recovery of SiMLR with the CCA energy and ICA source separation method. (b) Demonstrates performance of signal recovery of SiMLR with the CCA energy and SVD source separation method. (c) Demonstrates performance of signal recovery of SiMLR with the regression energy and ICA source separation method. The lower plots in (d) show how performance is impacted by the amount of matrix corruption. Here, lower scores are better. In this simulation study, SiMLR with CCA and SVD source separation does best in terms of both raw scores and pairwise test statistics.

- split the data into 80% training and 20% testing sets.
- in training data, we perform supervised dimensionality reduction where the 'omics data is jointly reduced with both death and survival time acting as a fourth matrix;
- train a Cox model with the low-dimensional bases derived from the 'omics data in the previous step;
- predict the survival outcome in test data and evaluate accuracy with the concordance metric.

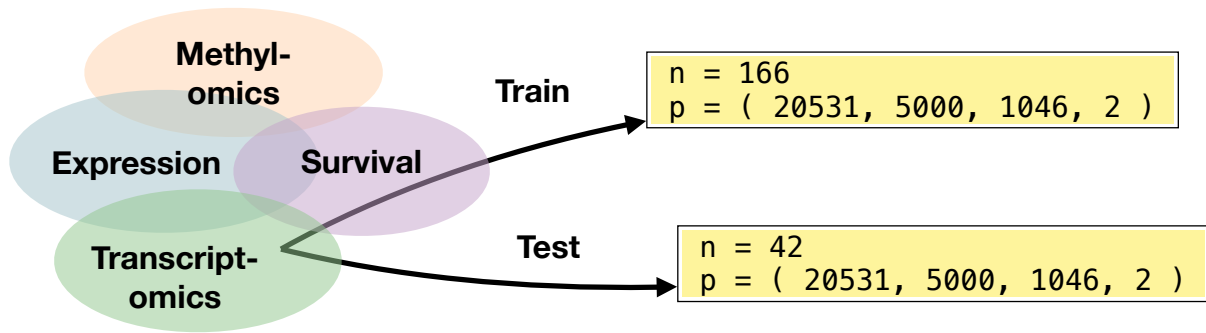
Under this design, a better method will both produce higher concordance values and produce more concordance values that meet or exceed the value of 0.6 which is considered a threshold of moderate agreement⁵³ and has been reported in recent studies for reasonably performing methods^{49,50}. We repeat the above experiments over 50 splits of the data in order to gain an empirical estimate of the difference in performance between SiMLR and SGCCA with different input data. We also test at three different sparseness levels thereby comparing the performance of solutions that yield feature vectors with low (25%), moderate (50%) and high (75%) sparseness.

In this evaluation, SiMLR with the reconstruction/regression energy shows an advantage over SGCCA in terms of predictive performance as measured by concordance in test data. Average concordance for SiMLR plus reconstruction is 0.64. The covariance energy and SGCCA perform nearly identically and, on average, do not exceed 0.6 concordance. Furthermore, in contrast to SGCCA, SiMLR's feature vectors are not only sparse but also smooth and unsigned (non-negative) which aids interpretation and may prevent overfitting, thus improving generalization. In the example code at `codeocean simlr_TCGA_survival.Rmd`, graph-based regularization parameters are selected to include 2.5% of the predictors in each predictor 'omics matrix (see the call to the `regularizeSimlr` function). As such, regularization is present but neither overwhelming nor optimized for this data. I.e. this value was chosen based on the desire for a small amount of denoising in the solution space. Neither method was optimized for this problem in terms of data selection, parameter or pre-processing choices. Moreover, the authors are not domain experts in this field. As such, this acts as a fairly unbiased comparison of these tools.

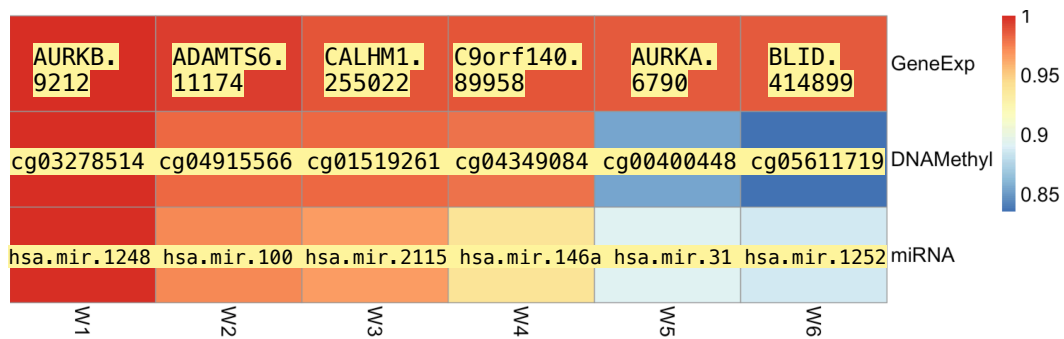
Figure 4 summarizes overall performance differences, along with the full output available on the `codeocean` platform. A brief summary of results is here for each comparison with pointers to the appropriate computational output file:

- [simlr_TCGA_survival_CCA_mix_ICA](#): SiMLR-CCA-ICA is compared to SGCCA at the three sparseness levels. At sparseness:
 - 0.25, a paired t -test shows $t = -1.04$, p -value = 0.30 (where positive t -statistic indicates better performance by SiMLR);
 - 0.50, a paired t -test shows $t = 1.01$, p -value = 0.32.
 - 0.75, a paired t -test shows $t = -1.41$, p -value = 0.16.
- [simlr_TCGA_survival_CCA_mix_SVD](#): SiMLR-CCA-SVD comparisons show:
 - at sparseness 0.25, $t = 0.72$, p -value = 0.48;
 - at sparseness 0.50, $t = 0.09$, p -value = 0.93;
 - at sparseness 0.75, $t = -0.82$, p -value = 0.41.
- [simlr_TCGA_survival_Reg_mix_ICA](#): SiMLR-Reg-ICA comparisons show:
 - at sparseness 0.25, $t = 4.53$, p -value = $3.74e-05$;
 - at sparseness 0.50, $t = 4.46$, p -value = $4.85e-05$;
 - at sparseness 0.75, $t = 1.81$, p -value = 0.08.
- [simlr_TCGA_survival_Reg_mix_SVD](#): SiMLR-Reg-SVD comparisons show:
 - at sparseness 0.25, $t = 4.14$, p -value = 0.0001;
 - at sparseness 0.50, $t = 3.61$, p -value = 0.0007;
 - at sparseness 0.75, $t = 2.55$, p -value = 0.0141.

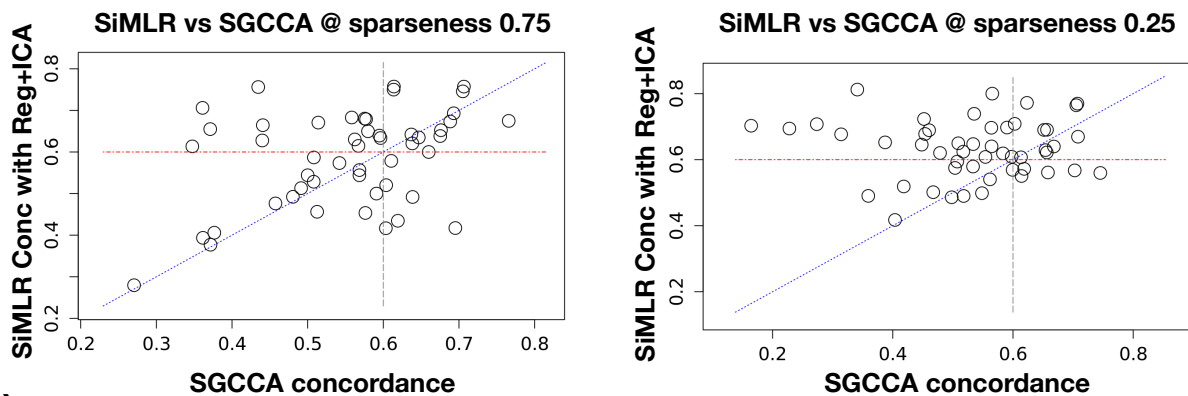
In summary, SiMLR with reconstruction performs statistically equivalently or better on average than SGCCA in this problem with SiMLR-Reg-ICA showing the best results over all sparseness values. SiMLR-CCA performed equivalently to SGCCA. In addition, as shown in Figure 4 (b), SiMLR provides feature weights that have a consistent sign and that allow the embeddings to be treated as weighted averages. This means that, for example, high values for gene expression-related embeddings are due to the contributions of individual genes that exhibit high expression levels. This aids interpretation of statistical models based on these embeddings because both the units and the directionality of these derived variables are clear.



(a)



(b)



(c)

Figure 4: Multi-omic study: supervised cancer survival prediction comparison to SGCCA. In (a), we show the train-test split numbers for each of the simulation runs as well as the n and p for each measurement type: gene expression, methylomics, transcriptomics and survival data. (b) Shows the most highly weighted (top 6) predictors selected for each of the modalities where the weights are normalized such that the maximum value is one. Because the feature vectors are non-negative, these lead to interpretable regression weights when the embeddings are combined with the Cox proportional-hazards model. (c) Shows plots of SiMLR concordance versus SGCCA concordance over all 50 runs. As such, points above the red dotted line and above the blue dotted line show where SiMLR performs reasonably and better than SGCCA. At left in (c) shows a case where SiMLR and SGCCA demonstrate close performance and (right) where SiMLR outperforms SGCCA the most.

2.5 SiMLR and SGCCA applied to PTBP brain age

The pediatric template of brain perfusion (PTBP⁵⁴) includes freely available multiple modality neuroimaging consistently collected in a cohort of subjects between ages 7 and 18 years of age. PTBP also includes a variety of demographic and cognitive measurements. A relevant reference analysis of this data is available in⁵⁵.

We provide pre-processed (machine learning ready) matrix format for three measurements taken in 97 subjects: voxelwise cortical thickness⁵⁶, fractional anisotropy (FA) derived from diffusion tensor imaging and cerebral blood flow (CBF) all at the voxel-wise level at 1mm resolution. The dimensionality of the matrices are $97 \times 515,317$ for thickness and CBF and $97 \times 438,394$ for FA. The development-related phenotype matrix consists of the subjects' sex, chronological age, total IQ score, verbal IQ score and performance IQ score. The IQ variables are highly correlated.

Figure 5 summarizes the design of the study. First, a 5-fold cross-validation grouping of subjects is defined. For each fold, SiMLR and SGCCA are run with parameters that are set to select interpretable “network”-like components. In this example, we choose these parameters specifically at higher sparseness levels to facilitate interpretability. We record computation time as well as the embedding vectors for each modality. We then train, within each fold, a linear regression model to predict age and IQ-related variables from the neuroimaging embeddings. This is a form of principal component regression. These predictions are stored for each fold to facilitate a final comparison of performance across all folds. We use this technique, rather than repeated resampling as in prior studies, in part because the run-time for this problem can be relatively long, up to 235 minutes for SGCCA. The following results are drawn from codeocean [simlr_PTBP_supervised_ICA](#) and [simlr_PTBP_supervised_SVD](#). The ICA and SVD differentiate which source separation method is used. Both show the SGCCA results and a summary of all cross-validated prediction is in the csv files called `simlr_ptbp_summary_results_ica` or `simlr_ptbp_summary_results_svd`.

2.5.1 Computation time

In this example, SGCCA and SiMLR run, on the `codeocean` platform, demonstrate overall similar run-time with a few exceptions. These exceptions are caused by data-dependent longer convergence times. SGCCA runs, over each of five folds, for 235, 29, 29, 30 and 33 minutes. SiMLR with CCA and ICA runs for 105, 46, 46, 41 and 46 minutes. SiMLR with CCA and SVD runs for 78, 58, 94, 53 and 56 minutes. SiMLR with regression and ICA runs for 44, 47, 55, 39 and 60 minutes. SiMLR with regression and SVD runs for 28, 31, 41, 54 and 33 minutes. Overall differences in run-time likely depend on convergence settings as well as the variability of the energy function combined with the input data.

2.5.2 Prediction outcomes

Figure 5 demonstrates the predictions' mean absolute error (MAE) for each algorithm that we tested:

- SGCCA yields 2.0 years MAE;

- SiMLR-Reg-SVD yields 1.70 years;
- SiMLR-CCA-ICA yields 1.64 years;
- SiMLR-Reg-ICA yields 1.58 years;
- SiMLR-CCA-SVD yields 1.44 years.

None of the methods perform well for predicting IQ-related scores. However, both SiMLR and SGCCA component regression produce reasonable predictions of brain age⁵⁷. These values reported here are competitive with those reported in⁵⁵. The MAE differences translate to a statistically significant improvement in performance between SiMLR (all variants) and SGCCA (best result p -value = 0.0002965, worst p -value = 0.04692). At the individual prediction level, this means that SiMLR produces a more accurate age in 61 of 97 cases for SiMLR-CCA-SVD.

2.6 SiMLR and SGCCA applied to imaging-genetics data

Pediatric Imaging, Neurocognition, and Genetics (PING) data⁵⁸ offers the opportunity to jointly study two types of neuroimaging, anxiety and depression related SNPs² and self-reported scores of anxiety and depression. The training portion of the data is defined by subjects who have only neuroimaging and SNPs. This allows us to perform dimensionality reduction in training subjects alone ($n=508$) to identify a much lower dimensional space that encodes the variability induced jointly by SNPs and brain structure. The test set is distinguished by individuals who have not only imaging and genetics measurements but also self-reported measures of anxiety and depression. We perform inference in the test set ($n=162$) to determine which, if any, of the learned embeddings relate to these scores.

The evaluation criterion, here, is inferential i.e. we prefer the method that leads to embeddings with greater relationship to the clinical scores. This exploratory study is shared in supplementary information. For this reason, we keep discussion, here, brief. Primarily, SiMLR identifies more signal related to anxiety and depression in the inferential portion of the study, when compared to SGCCA. I.e. more components relate to self-report anxiety and depression scores – with both SNPs and brain structure (thickness and white matter integrity, like PTBP) contributing – when using SiMLR compared to SGCCA. SiMLR leads to 3 components whereas SGCCA only identifies a single component related to anxiety. More importantly, however, we noted a severe difference in computation time. This study computes 40 components from high-dimensional data. SGCCA takes over 24 hours to compute these components. SiMLR (all variants) takes less than an hour. The primary difference between this study and the others included as examples is that the number of rows and the number of columns is relatively large (for training, $n=508$ and $p_{\text{thickness}} = 66, 565, p_2 = 68, 966, p_3 = 4, 309$). As such, the advantage SGCCA gains by working in the dual space may be overwhelmed by the combined cost of relatively large covariance matrices and the need to perform deflation for each set of components. In contrast, SiMLR computes the feature matrix for each modality in one pass through the optimization.

We also provide a related supplementary result in multi-omic Alzheimer’s disease neuroimaging initiative (ADNI) data. This result shows another way to relate imaging and cognition to genetic measurements: through polygenic risk measurements. Polygenic risk scores effectively reduce the dimensionality of genetic data based on an a priori weighted sum of trait-associated alleles. The supplementary study contrasts SiMLR, RGCCA and SGCCA applied to tabular data where $n \gg p$. The results of this joint reduction repeat trends shown elsewhere in this document; however, the difference between sparse and unconstrained dimensionality reduction is relatively less due to the more classical setting ($n \gg p$). This demonstrates that SiMLR can be used effectively, like RGCCA, even when a dataset is already relatively well-powered and does not suffer from the curse of dimensionality.

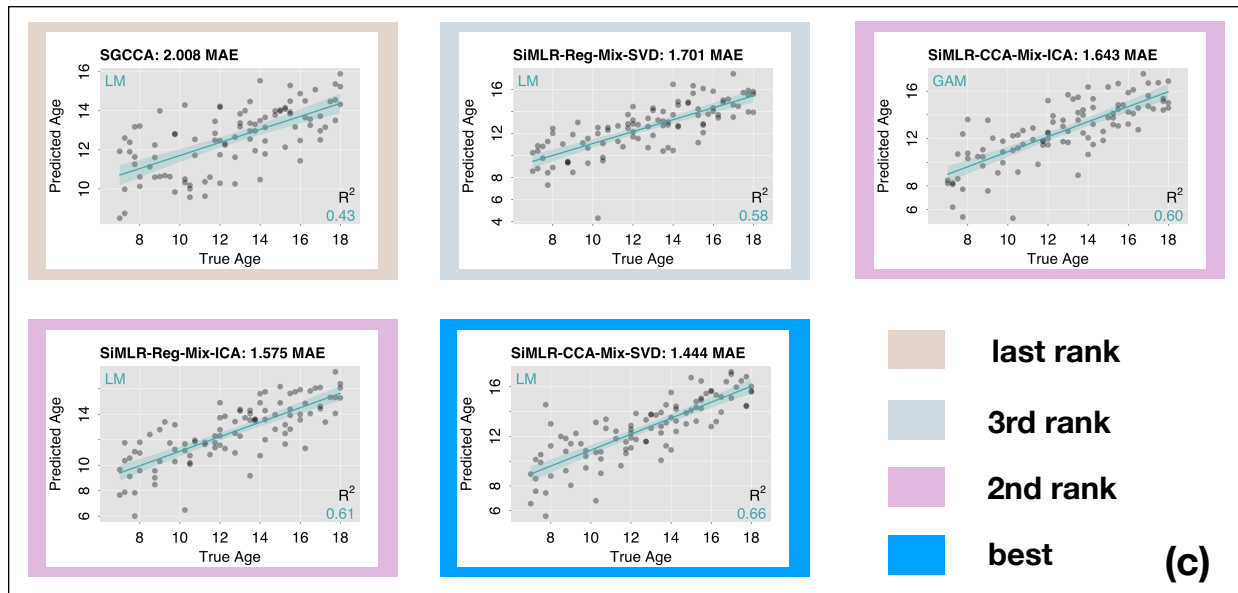
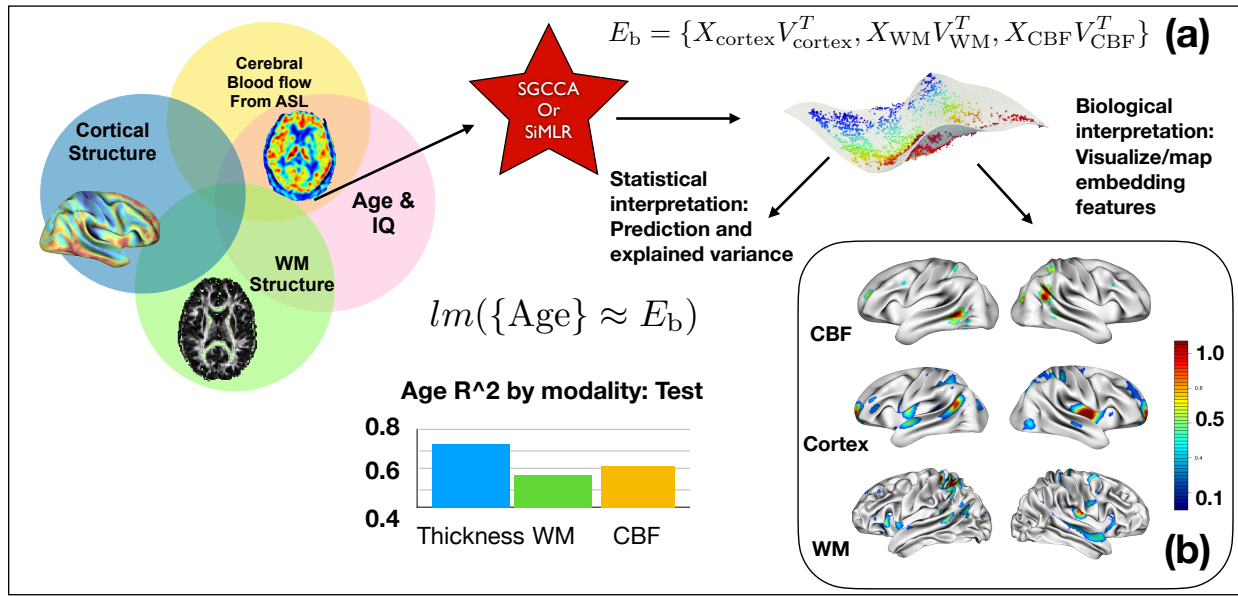


Figure 5: PTBP fully supervised brain age prediction: comparison to SGCCA. Brain age is the subject’s age predicted from neuroimaging data. Four matrices are input where cortical thickness, white matter integrity and cerebral blood flow derive from different types of neuroimages; the fourth modality describes brain maturation in terms of age and IQ measurements. Panel (a) shows the overall study design where embeddings are computed as in prior examples and then passed downstream to facilitate statistical and biological interpretation. The first phase of statistical interpretation (the bar plots) compares the ability of each modality to predict age independently and suggests thickness is most predictive (when acting alone); WM and CBF have close performance to each other (data drawn from best performing method). In (b), we show the feature vectors from the best performing method noting that the weights are relative to each feature vector where its values are scaled to zero to one. In (c) we show the ability to predict real age from the brain where SiMLR-CCA-SVD does best; none of the methods perform well for IQ prediction. Standard error bars are shown as gray shaded regions around a best-fit line. R^2 for the predicted model fit is also shown.

Table 1: Summary of RGCCA-SGCCA-SiMLR comparison results. The $x + / - y$ indicates mean and standard deviation values in the table below. RGCCA = regularized generalized canonical correlation analysis; SGCCA = sparse generalized canonical correlation analysis; Sim = similarity-driven multivariate linear reconstruction (SiMLR); Reg = regression; CCA = absolute canonical covariance; ICA = ICA blind source separation (BSS) method; SVD = SVD (BSS) method. Best results are highlighted in cadet blue; worst in antiquewhite. The second ranking approach is in pink. SiMLR with the absolute canonical covariance similarity measurement and SVD (SimCCASVD) as a BSS method performs best overall. For the multi-omics example, SiMLR with the regression energy and ICA BSS method (SimRegICA) outperforms SGCCA most consistently across sparseness levels, provides closely competitive performance overall, and is highlighted in pink. In brainAge, all SiMLR variants perform substantially better than SGCCA. The PING examples are exploratory analyses described in the supplementary information as we cannot directly share the data. The "n comp" description in the PING table refers to the number of significant components related to either anxiety or depression. The last row summarizes our overall ranking and explains the relationship of cell color to the ranking system. The rank is calculated by counting instances of a given rank across columns.

study	RGCCA	SGCCA	SimCCAICA	SimCCASVD	SimRegICA	SimRegSVD	metric
Signal-Sens.	0.35+/-0.18	0.45+/-0.17	0.5+/-0.15	0.51+/-0.14	0.49+/-0.13	0.49+/-0.14	R-squared
Noise-Sens.	0.09	0.16	0.09	0.06	0.07	0.1	R-squared
Multi-omic	N/A	0.56+/-0.12	0.56+/-0.13	0.56+/-0.14	0.64+/-0.08	0.64+/-0.11	Concordance
brainAge	N/A	2+/-1.5	1.6+/-1.2	1.4+/-1.2	1.6+/-1.3	1.7+/-1.2	MAE
PING-Anx	N/A	1 comp.	N/A	3 comp.	3 comp.	N/A	Inferential
PING-Dep	N/A	0 comp.	N/A	1 comp. (trend)	1 comp. (trend)	N/A	Inferential
Overall:	6th (worst)	5th	3rd	2nd	1st	4th	rank count

3 Discussion

This paper details SiMLR, an algorithm for computing interpretable embeddings from high-dimensional, multiple modality datasets. We demonstrate its performance in simulated data, in two examples on biomedical data and in one exploratory analysis on public data (in the supplementary results). SiMLR significantly outperforms RGCCA and its sparse variant SGCCA in the majority of these results. In a few cases, the method are statistically equivalent. The methods that we develop are generalizations of classical methods like PCA and CCA but exist within a single, consistently implemented framework. The implementation is efficient for high-dimensional data, builds in network-based regularization, extends to an arbitrary number of modalities and can be used for hypothesis testing, clustering or prediction studies. SiMLR was demonstrated and evaluated in studies relating imaging, genomics, cognition, demographics and other multi-omic datasets. We provide strategies for parameter setting, training and testing study design and the visualization and interpretation of results. The framework is open-source and relevant to understanding complex, potentially subtle patterns

in healthcare data.

Three supervised learning case studies demonstrate – with both code and datasets – how one may use SiMLR with either covariance related or regression related similarity measurements and with each source separation strategy. These examples are designed to show how scientists may adapt this tool for their own needs. We also recommend default choices for the similarity (reconstruction energy) and source separation (ICA) functions with the caveat that the outcomes presented in this manuscript may be dependent on the internal structure of these example datasets.

In our simulation study, SiMLR provides more robust signal recovery than other methods. Because this study is done in a training-testing format, these results are not due to over-fitting but due to the fact that SiMLR is able to uncover the ground truth result substantially more efficiently, as designed. This claim is supported by the fact that permutation results suggest no predictive signal can be learned (see online materials in `codeocean`). We note that both the SVD and ICA choices for the source separation algorithm achieve overall similar results. However, the best result is gained by the CCA-like energy combined with SVD as source separation method.

The simulation study also demonstrates the generative theory under which SiMLR operates. Consistent with the real biological data examples, SiMLR outperforms RGCCA/SGCCA in the simulation study. This may suggest that the simulation strategy is at least to some degree consistent with real data. Lastly, note that the importance of regularization for solving inverse problems is well-known at least since Tikhonov¹⁸.

The multi-omic cancer survival prediction study uses SiMLR as a tool for supervised feature learning. The learned embeddings are linked with Cox-hazard regression to predict survival in test data. SiMLR’s best performance in this data uses the reconstruction energy with ICA (or SVD) as source separation method and substantially exceeds SGCCA for most settings. However, we did note that SGCCA provided solutions with comparatively good performance for some parameter settings. SiMLR-Regression-ICA did overall best while SiMLR-CCA-SVD did worst. We hypothesize that this difference in performance may relate to the fact that the regression energy refers back to – in every gradient and similarity calculation – the full data matrix. CCA and similar criteria do not directly use the full data matrices in the energy assessment. Choice between the ICA and SVD source separation methods did not substantially impact performance for this problem; the energy function was overall more important.

These survival prediction outcomes highlight the importance of not only the selected method but also the data to which it is applied. That is, the best method for brainAge and in simulation was not the same as for survival prediction. Lastly, while these models produce average concordance values up to 0.64, they are not competitive with more traditional survival models. For example,⁵⁹ reports concordance results of 0.741, 95% CI: 0.714–0.768. However, these cohorts are not identical; more complete data would be required for a detailed and meaningful comparison.

The PTBP study uses SiMLR to perform supervised dimensionality reduction across four different datasets, three of which are high-dimensional neuroimaging and one of which is,

to the contrary, a low-dimensional development-related matrix. The feature vectors are learned in training data and then applied to brain age prediction in testing data. Relative to SGCCA, the SiMLR embeddings yield substantially better cross-validated performance across all settings. We attribute the advantage to both extra regularization and the direct primal optimization strategy.

Interestingly, in both simulation and real clinical data, SiMLR extracts different signal than SGCCA as judged by the systematic performance trends in these examples. This feature may relate to the method’s core mathematics: high-dimensional embedding vectors are constructed purely from within modality data but the low-dimensional bases are derived from cross-modality representations determined by a user-selected source separation algorithm. If the SVD source separation method is chosen, then this representation will be orthogonal; if ICA is chosen, they will be statistically independent where independence is defined by measuring non-gaussianity⁴⁰ (one of the tenets of fastICA is “non-gaussianity is independence”). This type of approach will only be effective in datasets that exhibit some degree of cross-modality covariation that can be decoded meaningfully into multiple “true” source signals. If this is not possible, then SiMLR may obscure rather than extract hidden signal.

Performance differences could relate to two other implementation details. SiMLR uses a primal formulation that directly optimizes in the high-dimensional feature space in which the energy function is defined. In contrast, SGCCA computes solution updates in a low-dimensional space (see Algorithm 1 in²⁶) and then performs soft-thresholding on the resulting vectors after transformation to the high-dimensional feature space. Secondly, SGCCA uses deflation to generate multiple components whereas SiMLR operates on full feature matrices. That is, SiMLR computes full matrix solutions all at once and uses the underlying source separation method to optimize these vectors jointly at each iteration of the algorithm. This improves computational efficiency when extracting several components (i.e. more than a few) but also marks a clear difference in the objective functions defined by SiMLR and SGCCA. These technical factors all contribute to differences in the outcomes reported here.

There are several limitations to this study and opportunities for future work. Primarily, we believe this approach and the current findings will be strengthened by application in related, larger datasets such as those provided by Adolescent Brain Cognitive Development (ABCD), the UK Biobank and Human Connectome Project. Furthermore, while we present methods for matrix standardization (the usual centering and scaling), this may not be a perfect solution for all cases, in particular when data deviates strongly from gaussianity. Other alternatives are available (e.g. rank transformations), but those are not explored here. While this work provides several automated or semi-automated strategies for selecting regularization parameters and the rank (k) for the feature vectors, none of these strategies are “perfect”. This is unsurprising, given that technical research continues about parameter setting even in more classical methodology (PCA, CCA). While cross-validation approaches may also be used, the computational and data expense for these is relatively high and they also suffer theoretical as well as practical limitations in terms of effectiveness⁶⁰. Despite these issues that are rather general, we believe the current implementation and interface to SiMLR, combined with guidance provided here, may yield a practically useful tool for multiple modality analysis of biomedical imaging and related data.

A second caveat to this study is that the design is explicitly multivariate and, as such, we do not interrogate the predictive value of individual embeddings. Our statistical focus is on the omnibus models. Other researchers may prefer to study individual embeddings independently. This is one known limitation within the current demonstration of SiMLR. Future work may explore this research in conjunction with extracting not just joint but also individual structure. This latter advantage is one provided by JIVE. SiMLR could also be further optimized directly for clustering problems, e.g. by implementing a multi-view clustering loss^{61,62}.

Two technical findings from these results are suggestive of directions for future work. First, SiMLR’s performance suggests that a primal formulation for large joint matrix learning problems is feasible and can achieve competitive results in real and simulated data. Second, direct computation of feature matrices (vs. feature vectors as is done with deflation schemes) provides computational advantages in our experiments. However, further analysis of the differences between these technical approaches within a consistent framework would be needed to draw deeper conclusions.

Beyond the formulation and implementation of the method, accessibility of the algorithm is a key contribution. `ANTsR` is available in `GitHub` and via the `neuroconductor` software distribution platform. Thus, SiMLR is available for near immediate access to users who are familiar with the R computing environment and who wish to test its applicability in their own data. As always, we recommend interested users contact developers/authors for guidance or with issues arising in the use of this software.

4 Acknowledgments

This work is supported by the Office of Naval Research N00014-18-1-2440 and K01-ES025432-01. Correspondence and request for materials should be directed to Dr. Avants.

5 Author contributions

B.B.A. and N.J.T. and J.R.S made substantial contributions to the conception and design of the work and the analysis and interpretation of data; all authors drafted the work and revised it.

B.B.A. and N.J.T. created the new software used in the work.

6 Methods

6.1 Software platform: `ANTsR`

The core platform, `ANTsR`, leverages the powerful R language to interface and help organize raw neuroimaging, genomics and other data. `ANTsR` uses `Rcpp`⁶³ to wrap Insight ToolKit (ITK, now in version 5⁶⁴) and ANTs (currently in version 2.3.3⁶⁵) C++ tools for the R environment. `ANTsR` is accessible via both `GitHub` and `neuroconductor`⁶⁶ and is currently in version v0.5.7.4.

Test data and readme files are available by typing `?simlr` from within ANTsR. The software used for this paper is available at [the ANTsR GitHub repository](#).

6.2 Technical background

We discuss, briefly, the primary algorithms upon which SiMLR is based. We assume data matrices, below, are standardized (columns with zero mean, unit variance) and $\|\cdot\|$ denotes the Frobenius norm.

6.2.1 Multiple regression

Multiple regression solves a least squares problem that optimally fits several predictors (the $n \times p$ matrix X) to an outcome (y). As a quadratic minimization problem, we have:

$$\arg \min_{\beta} \|y - X\beta\|^2,$$

with optimal least squares solution:

$$\hat{\beta} = (X^T X)^{-1} X^T y.$$

Above, we may also add a “ridge” penalty $\lambda\|\beta\|^2$ on the β s which is useful if $p \gg n$ i.e. in the case of complex, multi-view, and multivariate datasets as we propose to model here. In this document, n refers to the number of samples or subjects and p to predictors.

6.2.2 Principal component analysis

PCA, like multiple regression, may be formulated as the solution to an energy minimization problem. Select $k < n$, then find U ($n \times k$), V ($p \times k$) that minimize reconstruction error (where we add an ℓ_1 constraint as in⁶⁷⁻⁶⁹ to illustrate sparse PCA):

$$\arg \min_{U,V} \|X - UV^T\|^2 + \sum_k \lambda_k \|V_k\|_1,$$

with additional constraints $U = XV$ and $V^T V = I$ where I is the identity matrix. The details of these constraints may vary in regularized variants of the method. Each of the columns of X is, here, expressed as a linear combination of the columns of U . For several modalities, we would compute: $\{X_1 = U_1 V_1^T, \dots, X_n = U_n V_n^T\}$. In this case, the “predictors” are the U_i and the V_i is analogous to the β in the multiple regression case. The V_i feature vectors will be sparse if the ℓ_0 or ℓ_1 penalty is used.

6.2.3 Canonical correlation analysis

CCA may be thought of as a generalization of multiple regression. Denoting Y as a $n \times q$ matrix, CCA seeks to find solution matrices $U(k \times p)$, $V(k \times q)$ that maximize correlation in a low-dimensional space between X and Y :

$$\arg \max_{U,V} \text{tr}(\text{Corr}(XU^T, YV^T)),$$

where $Corr$ is Pearson correlation and tr is the trace operator. In contrast to our previous formulation for PCA, CCA evaluates the objective function (the “energy”) in a reduced dimensionality space. Any of the methods above can be made sparse by enforcing the penalties on the feature weights as described for sparse PCA with the caveat that optimality constraints must be relaxed. Non-convex optimization methods such as alternating minimization and/or projected gradient descent must then be used^{70–72}.

6.3 Similarity-driven multi-view linear reconstruction

SiMLR is a general framework that can be specified in forms that relate to either sparse PCA (a regression-like objective) or sparse CCA (a covariance-related objective). The primary concepts are illustrated in Figure 1. We make two assumptions about datasets to which we will apply SiMLR.

- **Assumption 1:** Real latent signal(s) are independent and linearly mixed across the biological system on which we are collecting several measurements (a standard assumption for blind source separation).
- **Assumption 2:** Sparse, regularized feature vectors can relate estimated latent signals in assumption 1 to the original data matrices through linear operations.

If data matches these assumptions then methods that can combine modalities have a better chance of finding the latent signals; e.g. joint analysis from (for example) genetics, neuroimaging and cognition may provide more reliable recovery of the true latent signal influencing them all. Furthermore, it is likely that spurious signal will not be shared across all modalities – or all elements of the features within a modality – in a consistent manner. Natural filtering of noise occurs in joint analysis because (most forms of) noise does not covary across measurement instances. Adding regularization goes further in adding robustness: methods regularized with sparseness terms (ℓ_0 or ℓ_1) can down-weight (even to zero) features that do not improve the objective function. A caveat of these assumptions is that if no covariation across measurements exists – or if noise overwhelms all modalities/measurements – then these methods may not be relevant.

6.3.1 The SiMLR objective function

We first present the high-level framework and will expand upon details for similarity measurement and regularization below. The core concepts in SiMLR include the fact that it incorporates flexible approaches to measuring differences between modalities (similarity-driven), can take as input several different matrices (multi-view) and that all operations are linear algebraic in nature (linear reconstruction). First, we define X_i as a $n \times p_i$ (subjects by features) matrix for a given measurement/view/modality. The i ranges from 1 to m i.e. the number of modalities (or views). Then SiMLR optimizes an objective function that seeks to approximate each modality from its partner matrices through a sparse feature matrix (V_i) and low-dimensional representations ($U_{\neq i}$):

$$\arg \min_{V_i} \sum_{i=1}^m S(X_i, f(U_{\neq i}), V_i) + \text{Regularization}(V_i),$$

where:

- k denotes the rank of V_i and U_i ;
- V_i is a $p_i \times k$ matrix of feature/solution vectors (analogous to β s) for the X_i modality;
- $\forall_i U_i = X_i V_i$;
- $U_{\neq i}$ is a $n \times (k(m-1))$ low-dimensional representation of modalities other than X_i i.e. the column-bound matrix $U_{\neq 2} = [U_1, U_3]$ if $i = 2$ and $m = 3$;
- f is a function (with output dimensionality $n \times k$) that estimates a low-rank basis set from its argument, is related to **Assumption 1**, and is described in more detail below;
- S is a function measuring the quality of the approximation of X_i from the other modalities and is related to **Assumption 2**;

The $f(U_{\neq i}) = \tilde{U}_{\neq i}$ is a key novel component in the SiMLR framework and is derived by performing blind source separation over the set of $j \neq i : \{X_j V_j\}$ embeddings (the $U_{\neq i}$). We now provide details for each term and other aspects of the implementation.

Similarity Options. The default similarity measurement is one of difference. This is akin to the reconstruction form for PCA, discussed above. In this case, we have:

$$S(X_i, \tilde{U}_{\neq i}, V_i) = \|X_i - \tilde{U}_{\neq i} V_i^T\|^2.$$

Here, SiMLR attempts to reconstruct – in a least-error sense – each matrix X_i directly from the basis representation of the other $n - 1$ modalities.

We also implement a similarity term inspired by CCA but modified for the SiMLR objective function. In prior work, we observed that the CCA criterion – in the under-constrained form here where we expect $p \gg n$ – demonstrates some sensitivity to the sign of correlations⁷³. As such, we implement an absolute canonical covariance (ACC) similarity measurement expressed as:

$$\frac{\text{tr}(| \tilde{U}_{\neq i}^T X_i V_i |)}{\|\tilde{U}_{\neq i}\| \|X_i V_i\|}.$$

Both reconstruction and ACC have easily computable analytical derivatives that are amenable to projected gradient descent, as used in our prior work^{11,12,17}. This similarity term is most closely related to SABSCOR and SABSCOV in multi-block data analysis^{74,75}. However, it focuses only on cross-modality signal.

For the reconstruction energy, SiMLR optimizes these feature vectors to reconstruct each full matrix from a reduced representation of the other matrices (the $\tilde{U}_{\neq i}$). For ACC, SiMLR optimizes V_i to maximize covariance of $X_i V_i$ with the low-rank basis. As such, the latter

similarity term may be more appropriate for recovering signal that exists more sparsely in the input matrices. This is because the operation $X_i V_i$ is able to completely ignore large portions of the given matrix X_i due to the sparseness terms in our regularization (described below). The regression energy, on the other hand, will be more directly informed by the raw high-dimensional matrix which may have advantages in some cases. Quadratic energies also tend to have larger capture ranges.

The method’s performance also depends on the selection for the basis representation. We evaluate two options in this initial work:

- $f_{svd} = svd_u([U_{\neq i}])$
- $f_{ica} = ica_S([U_{\neq i}])$

The notation $[U_{\neq i}]$ indicates that we bind the columns together (**cbind** in R). Below *alg* will represent svd_u or ica_S . The method ica_S indicates that we take the independent components matrix (the S matrix) from the ICA algorithm (where ICA produces $X = AS$). The method svd_u indicates that we take the U component of the SVD (where SVD produces $X = UDV^T$).

We focus our evaluation on ica_S and svd_u functions in this work as we have found that they produce useful outcomes in example experiments and they are well-proven methods applied in several domains. The assumptions underlying ICA and SVD are related. They both fit our assumption 1 above of linearly mixed independent signals. The difference is the measure of independence. SVD (or PCA) assumes independence is measured by variance which leads to orthogonal basis functions. ICA uses non-gaussianity to measure independence. Both are valid options, from the theoretical perspective, and we rely on evaluation results to make recommendations about how to choose between these in practice.

Regularization options. Regularization occurs on the V_i i.e. our feature matrices. Denote:

- v_{ik} as the the k^{th} feature vector in V_i ;
- G_i is $p_i \times p_i$ a sparse regularization matrix with rows that sum to one;
- γ_i as a scalar weight which could be used to regularize each component differently; effectively, this controls the sparseness and varies in zero to one.

Then the regularization terms take the form:

$$\text{Regularization}(V_i) = \sum_i \sum_k \gamma_i \|G_i v_{ik}\|_{\ell_p}^+,$$

where $\|\cdot\|_{\ell_p}^+$ is the positivity constrained ℓ_p norm (usually, $p = 0$ or $p = 1$). This term both enforces sparseness via ℓ_p while providing data-adaptive degrees of smoothing via the the graph regularization matrix G^i . For neuroimaging, this latter feature means that one does not need to pre-smooth images before running SiMLR. In practice, $\|\cdot\|_{\ell_p}^+$ induces unsigned feature vectors. I.e. all non-zero entries will be either only positive or only negative.

Regularization weights: The parameterization of the sparseness for each modality is set by γ_i in the range of zero to one, where higher values are increasingly sparse (more values of

the feature vector are zero). By default, γ_i is automatically set to accept the largest 50th percentile weights but the user may decide to increase or decrease this value depending on the needs of a specific study. Alternatively, one may use hyperparameter tuning methods to automatically determine γ_i . For most applications, we recommend default values.

Regularization matrices: optional G_i are currently set by the user and must be determined in a data/application/hypothesis-specific manner. In implementation, we provide helper functions that allow the user to employ k -nearest neighbors (KNN) to set the (potentially large) regularization matrices. We use HNSW⁷⁶ to compute sparse KNN matrix representations for the G_i . HNSW is among the most efficient methods currently available and, combined with sparse matrix representations, make graph regularization on large input matrices efficient. This aspect of regularization promotes smooth feature vectors where the nature of smoothness is typically determined by proximity either spatially or in terms of feature magnitude or feature correlation.

Although we provide default methods, choice of regularization should involve some consideration on the part of the user. Because there is no single theoretically justified answer to these questions, the best general approach would be to use hyper-parameter optimization. Alternatively, domain-specific knowledge may be used to guide parameter setting, in particular sparseness and regularization. Rules of thumb should be, for regularization, that the estimated V_i should appear to reflect biologically plausible feature sets. For sparseness, biological plausibility should also be considered although we believe our default parameters provide good general performance. As such, regularization (i.e. construction of the G_i) should perhaps be given more domain-dependent attention by users. Examples below provide clarity on how we set these terms in practice. E.g. in neuroimaging, we may use $k = 5^d$ mask-constrained neighbors for KNN where d is image dimensionality. For genomics or psychometrics data, we may set regularization simply by thresholding correlation (or [linkage disequilibrium](#)⁷⁷) matrices.

6.4 SiMLR: Optimization

The overall approach to optimizing the SiMLR objective is that of projected gradient descent⁷⁸. In this context, one derives the optimization algorithm without regularization constraints and then, at each iteration, projects to the sub-space defined by the regularization terms. The SiMLR objective function for V_i , at a given iteration, depends only on the set values for X_i and $\tilde{U}_{\neq i}$. As such, we only need the gradient of the similarity term with respect to V_i which greatly simplifies implementation. We optimize total energy E via a projected gradient descent algorithm:

$$\begin{aligned} & \text{loop until convergence:} \\ \forall_i V_i^{\text{new}} & \leftarrow H(G_i \star (V_i - \partial S / \partial V_i \epsilon_i)) \\ \forall_i \tilde{U}_{j \neq i} & \leftarrow f_{alg}([X_j V_j^{\text{new}}]_{\neq i}) \end{aligned}$$

where:

- $[X_j V_j^{\text{new}}]_{\neq i}$ is the collection of low-dimensional projections resulting from multiplying the feature vectors onto the data matrices where $\neq i$ indicates that the i^{th} projection is held out;
- H is the thresholding operation which here is applied separately to each column of V_i (see the iterative hard/soft thresholding literature⁷² and⁷⁸ which suggests that ℓ_0 penalties provide greater robustness to noise);
- ϵ_i is a gradient step parameter determined automatically by line-search over the total energy E .

Recall that f_{alg} is a dimensionality reduction step that reduces $U_{\neq i}$ to a k -column matrix. Here, we provide an example gradient calculation for our default reconstruction error:

$$S = \|X_i - \tilde{U}_{\neq i} V_i^T\|^2,$$

$$\partial S / \partial V_i = -2(X_i^T - V_i \tilde{U}_{\neq i}^T) \tilde{U}_{\neq i},$$

which allows updating the full V_i at each gradient step. SiMLR only allows gradient-based updates that improve the total energy; these are arrived at by line search over the gradient step size and means that the objective function (driven primarily by the similarity term) is improved by the new candidate solution; this process is iterated until the method reaches a fixed point. A fixed point is – practically speaking – a convergent solution. I.e. if we further iterate the algorithm, the solutions do not change beyond some small numeric fluctuation.

This strategy also allows SiMLR to work directly on the feature matrices themselves even when $p \gg n$. When large numbers of components are being computed, this can lead to a distinct computational advantage in comparison to deflation methods.

6.5 SiMLR: Parameters and initialization

We summarize default (recommended) parameters and preprocessing steps for the methodology.

- Matrix pre-processing is performed automatically. Unless the user overrides default behavior, we transform each matrix such that: $\forall X_i : X_i \leftarrow \frac{sc(X_i)}{np_i}$ where sc denotes scaling and centering applied to the matrix columns. Normalizing by np controls the relative scale of the eigenvalues of each matrix.
- Number of components (k) – The practice for setting these values is very similar to practice in PCA or SVD; it may be determined via statistical power considerations, cross-validation or set to be $k = n - 1$, one less than the number of subjects. This is a problem that is currently under active research⁶⁰.
- Similarity measurement – evaluation and comparison of similarity choices is ongoing. Trade-offs are comparable to choosing correlation versus Euclidean distance for vectors and better performance may be gained in a data-dependent manner. ACC is faster to compute on a per-iteration basis but may require more iterations to converge. This

latter comment is an empirical observation based on our studies which, again, may be data dependent.

- Source separation algorithm – Trade-offs are comparable to choosing between SVD and ICA in general. Effectively, ICA should force the multiple component solutions toward statistical independence in a non-gaussian sense. SVD would be more appropriate for separating purely gaussian sources that are mixed linearly.

The nature of the feature space is impacted by the constraints on the U_i which are determined by the user-selected source separation algorithm. SVD produces an orthogonal latent space whereas ICA does not. ICA seeks a latent space that demonstrates statistical independence, that is, that are maximally non-gaussian^{40,41}. It is an empirical question about which is “best” for a given dataset; neither is right or wrong in an absolute sense. SVD and ICA are both used in many practical applications in machine learning and statistics. Our experiments confirm that both options can produce results that outperform RGCCA. Overall, the reconstruction error with ICA source separation appears to give good general performance in our experiments.

SiMLR may be initialized with several different approaches:

- random matrices for all or for each individual modality;
- a joint ICA or SVD across concatenated modalities (recommended and default behavior);
- Any other initial low-rank basis set e.g. derived from RGCCA, etc which may be passed to the algorithm by the user;

Due to the fact that SiMLR cannot guarantee convergence to a global optimum (sparse selection is a NP-hard problem), several different starting points should be evaluated when using SiMLR in new problems. This is in concordance with the theory of **multi-start** global optimization which we can only approximate in practice^{79,80}. Other joint reduction methods such as SGCCA suffer the same limitation. Our recommended default behavior avoids forcing users to explore multiple starting points but does not eliminate this fundamental issue that is general to the field of feature selection in high-dimensional spaces.

References

1. Cole, J. H., Marioni, R. E., Harris, S. E. & Deary, I. J. Brain age and other bodily ‘ages’: implications for neuropsychiatry. (2019) doi:[10.1038/s41380-018-0098-1](https://doi.org/10.1038/s41380-018-0098-1).
2. Wray, N. R. et al. Genome-wide association analyses identify 44 risk variants and refine the genetic architecture of major depression. Nature Genetics (2018) doi:[10.1038/s41588-018-0090-3](https://doi.org/10.1038/s41588-018-0090-3).
3. Habeck, C., Stern, Y. & Alzheimer’s Disease Neuroimaging Initiative. Multivariate data analysis for neuroimaging data: overview and application to Alzheimer’s disease. Cell Biochem Biophys **58**, 53–67 (2010).
4. Shamy, J. L. et al. Volumetric correlates of spatiotemporal working and recognition memory impairment in aged rhesus monkeys. Cereb Cortex **21**, 1559–1573 (2011).
5. McKeown, M. J. et al. Analysis of fMRI data by blind separation into independent spatial components. Hum Brain Mapp **6**, 160–188 (1998).
6. Calhoun, V. D., Adali, T., Pearlson, G. D. & Pekar, J. J. A method for making group inferences from functional {MRI} data using independent component analysis. Hum Brain Mapp **14**, 140–151 (2001).
7. Calhoun, V. D., Liu, J. & Adali, T. A review of group {ICA} for f{MRI} data and {ICA} for joint inference of imaging, genetic, and {ERP} data. Neuroimage **45**, S163–72 (2009).
8. Avants, B. Relating high-dimensional structural networks to resting functional connectivity with sparse canonical correlation analysis for neuroimaging. vol. 136 (2018).
9. Pierrefeu, A. de et al. Structured Sparse Principal Components Analysis With the TV-Elastic Net Penalty. IEEE transactions on medical imaging **37**, 396–407 (2018).
10. Du, L. et al. Structured sparse canonical correlation analysis for brain imaging genetics: an improved GraphNet method. Bioinformatics (Oxford, England) **32**, 1544–1551 (2016).
11. Avants, B. et al. Sparse unbiased analysis of anatomical variance in longitudinal imaging. vol. 6361 LNCS (2010).
12. Avants, B. et al. Sparse canonical correlation analysis relates network-level atrophy to multivariate cognitive measures in a neurodegenerative population. NeuroImage **84**, (2014).
13. Du, L. et al. GN-SCCA: Graphnet based sparse canonical correlation analysis for brain imaging genetics. in Lecture notes in computer science (including subseries lecture notes in artificial intelligence and lecture notes in bioinformatics) (2015). doi:[10.1007/978-3-319-23344-4_27](https://doi.org/10.1007/978-3-319-23344-4_27).
14. Guigui, N. et al. Network regularization in imaging genetics improves prediction performances and model interpretability on Alzheimer’s disease. in Proceedings - international symposium on biomedical imaging (2019). doi:[10.1109/ISBI.2019.8759593](https://doi.org/10.1109/ISBI.2019.8759593).
15. Lee, D. D. & Seung, H. S. Learning the parts of objects by non-negative matrix factorization. Nature (1999) doi:[10.1038/44565](https://doi.org/10.1038/44565).

16. Chalise, P. & Fridley, B. L. Integrative clustering of multi-level 'omic data based on non-negative matrix factorization algorithm. PLoS ONE (2017) doi:[10.1371/journal.pone.0176278](https://doi.org/10.1371/journal.pone.0176278).
17. Dhillon, P. et al. Subject-specific functional parcellation via Prior Based Eigenanatomy. NeuroImage **99**, (2014).
18. Tikhonov, A. N. On the stability of inverse problems. Doklady Akademii Nauk Sssr (1943).
19. Bell, J. B., Tikhonov, A. N. & Arsenin, V. Y. Solutions of Ill-Posed Problems. Mathematics of Computation (1978) doi:[10.2307/2006360](https://doi.org/10.2307/2006360).
20. Smilde, A. K., Westerhuis, J. A. & De Jong, S. A framework for sequential multiblock component methods. Journal of Chemometrics (2003) doi:[10.1002/cem.811](https://doi.org/10.1002/cem.811).
21. Tenenhaus, A. & Tenenhaus, M. Regularized Generalized Canonical Correlation Analysis. Psychometrika (2011) doi:[10.1007/s11336-011-9206-8](https://doi.org/10.1007/s11336-011-9206-8).
22. Tenenhaus, M., Tenenhaus, A. & Groenen, P. J. Regularized Generalized Canonical Correlation Analysis: A Framework for Sequential Multiblock Component Methods. Psychometrika (2017) doi:[10.1007/s11336-017-9573-x](https://doi.org/10.1007/s11336-017-9573-x).
23. Zhan, Z., Ma, Z. & Peng, W. Biomedical Data Analysis Based on Multi-view Intact Space Learning with Geodesic Similarity Preserving. Neural Processing Letters **1** (2018) doi:[10.1007/s11063-018-9874-9](https://doi.org/10.1007/s11063-018-9874-9).
24. Baltrusaitis, T., Ahuja, C. & Morency, L. P. Multimodal Machine Learning: A Survey and Taxonomy. (2018) doi:[10.1109/TPAMI.2018.2798607](https://doi.org/10.1109/TPAMI.2018.2798607).
25. Kettenring, J. R. Canonical analysis of several sets of variables. Biometrika (1971) doi:[10.1093/biomet/58.3.433](https://doi.org/10.1093/biomet/58.3.433).
26. Tenenhaus, A. et al. Variable selection for generalized canonical correlation analysis. Biostatistics (2014) doi:[10.1093/biostatistics/kxu001](https://doi.org/10.1093/biostatistics/kxu001).
27. Rohart, F., Gautier, B., Singh, A. & Lê Cao, K. A. mixOmics: An R package for 'omics feature selection and multiple data integration. PLoS Computational Biology (2017) doi:[10.1371/journal.pcbi.1005752](https://doi.org/10.1371/journal.pcbi.1005752).
28. Garali, I. et al. A strategy for multimodal data integration: Application to biomarkers identification in spinocerebellar ataxia. Briefings in Bioinformatics (2017) doi:[10.1093/bib/bbx060](https://doi.org/10.1093/bib/bbx060).
29. Arnaud Gloaguen, Cathy Philippe, Vincent Frouin, Giulia Gennari, Ghislaine Dehaene-Lambertz, Laurent Le Brusquet, A. T. Multiway Generalized Canonical Correlation Analysis. Biostatistics In Press, (2020).
30. Hotelling, H. Canonical Correlation Analysis (CCA). J. Educ. Psychol. (1935).
31. Hotelling, H. Relations between two sets of variants. Biometrika 321–377 (1936).
32. Lock, E. F., Hoadley, K. A., Marron, J. S. & Nobel, A. B. Joint and individual variation explained (JIVE) for integrated analysis of multiple data types. Annals of Applied Statistics

(2013) doi:[10.1214/12-AOAS597](https://doi.org/10.1214/12-AOAS597).

33. Yu, Q., Risk, B. B., Zhang, K. & Marron, J. S. JIVE integration of imaging and behavioral data. NeuroImage (2017) doi:[10.1016/j.neuroimage.2017.02.072](https://doi.org/10.1016/j.neuroimage.2017.02.072).
34. Ceulemans, E., Wilderjans, T. F., Kiers, H. A. & Timmerman, M. E. MultiLevel simultaneous component analysis: A computational shortcut and software package. Behavior Research Methods (2016) doi:[10.3758/s13428-015-0626-8](https://doi.org/10.3758/s13428-015-0626-8).
35. Argelaguet, R. et al. Multi-Omics Factor Analysis—a framework for unsupervised integration of multi-omics data sets. Molecular Systems Biology (2018) doi:[10.15252/msb.20178124](https://doi.org/10.15252/msb.20178124).
36. Carmichael, I. et al. Joint and individual analysis of breast cancer histologic images and genomic covariates. arXiv preprint [arXiv:1912.00434](https://arxiv.org/abs/1912.00434) (2019).
37. McMillan, C. et al. White matter imaging helps dissociate tau from TDP-43 in frontotemporal lobar degeneration. Journal of Neurology, Neurosurgery and Psychiatry **84**, (2013).
38. McMillan, C. et al. Genetic and neuroanatomic associations in sporadic frontotemporal lobar degeneration. Neurobiology of Aging **35**, (2014).
39. Cook, P. et al. Relating brain anatomy and cognitive ability using a multivariate multimodal framework. NeuroImage **99**, (2014).
40. Hyvärinen, A. & Oja, E. Independent component analysis: A tutorial. Notes for International Joint Conference on Neural Networks (IJCNN'99), Washington DC (1999).
41. Hyvärinen, A. & Oja, E. Independent component analysis: Algorithms and applications. Neural Networks (2000) doi:[10.1016/S0893-6080\(00\)00026-5](https://doi.org/10.1016/S0893-6080(00)00026-5).
42. De Vito, R., Bellio, R., Trippa, L. & Parmigiani, G. Multi-study factor analysis. Biometrics (2019) doi:[10.1111/biom.12974](https://doi.org/10.1111/biom.12974).
43. Haykin, S. & Chen, Z. The cocktail party problem. (2005) doi:[10.1162/0899766054322964](https://doi.org/10.1162/0899766054322964).
44. Goodwin, S., McPherson, J. D. & McCombie, W. R. Coming of age: Ten years of next-generation sequencing technologies. (2016) doi:[10.1038/nrg.2016.49](https://doi.org/10.1038/nrg.2016.49).
45. Yong, W. S., Hsu, F. M. & Chen, P. Y. Profiling genome-wide DNA methylation. (2016) doi:[10.1186/s13072-016-0075-3](https://doi.org/10.1186/s13072-016-0075-3).
46. Ozsolak, F. & Milos, P. M. RNA sequencing: Advances, challenges and opportunities. (2011) doi:[10.1038/nrg2934](https://doi.org/10.1038/nrg2934).
47. Andersen, P. K. & Gill, R. D. Cox's Regression Model for Counting Processes: A Large Sample Study. The Annals of Statistics (1982) doi:[10.1214/aos/1176345976](https://doi.org/10.1214/aos/1176345976).
48. Fox, J. & Weisberg, S. Cox Proportional-Hazards Regression for Survival Data in R. Most (2011).
49. Huang, L. et al. Development and validation of a prognostic model to predict the prognosis of patients who underwent chemotherapy and resection of pancreatic adenocarcinoma: A

large international population-based cohort study. BMC Medicine (2019) doi:[10.1186/s12916-019-1304-y](https://doi.org/10.1186/s12916-019-1304-y).

50. Neums, L., Meier, R., Koestler, D. C. & Thompson, J. A. Improving survival prediction using a novel feature selection and feature reduction framework based on the integration of clinical and molecular data. in Pacific symposium on biocomputing (2020). doi:[10.1142/9789811215636_0037](https://doi.org/10.1142/9789811215636_0037).

51. Rappoport, N. & Shamir, R. Multi-omic and multi-view clustering algorithms: review and cancer benchmark. Nucleic Acids Research (2018) doi:[10.1093/nar/gky889](https://doi.org/10.1093/nar/gky889).

52. Witten, D. M., Tibshirani, R. & Hastie, T. A penalized matrix decomposition, with applications to sparse principal components and canonical correlation analysis. Biostatistics (2009) doi:[10.1093/biostatistics/kxp008](https://doi.org/10.1093/biostatistics/kxp008).

53. Barnhart, H. X., Haber, M. & Song, J. Overall concordance correlation coefficient for evaluating agreement among multiple observers. (2002) doi:[10.1111/j.0006-341X.2002.01020.x](https://doi.org/10.1111/j.0006-341X.2002.01020.x).

54. Avants, B. B. et al. The pediatric template of brain perfusion. Scientific data (2015) doi:[10.1038/sdata.2015.3](https://doi.org/10.1038/sdata.2015.3).

55. Kandel, B., Wang, D., Detre, J., Gee, J. & Avants, B. Decomposing cerebral blood flow MRI into functional and structural components: A non-local approach based on prediction. NeuroImage **105**, (2015).

56. Tustison, N. et al. Logical circularity in voxel-based analysis: Normalization strategy may induce statistical bias. Human Brain Mapping **35**, (2014).

57. Franke, K. & Gaser, C. Ten years of brainage as a neuroimaging biomarker of brain aging: What insights have we gained? (2019) doi:[10.3389/fneur.2019.00789](https://doi.org/10.3389/fneur.2019.00789).

58. Jernigan, T. L. et al. The Pediatric Imaging, Neurocognition, and Genetics (PING) Data Repository. NeuroImage (2016) doi:[10.1016/j.neuroimage.2015.04.057](https://doi.org/10.1016/j.neuroimage.2015.04.057).

59. Manola, J. et al. Prognostic model for survival in patients with metastatic renal cell carcinoma: Results from the international kidney cancer working group. Clinical Cancer Research (2011) doi:[10.1158/1078-0432.CCR-11-0553](https://doi.org/10.1158/1078-0432.CCR-11-0553).

60. Bro, R., Kjeldahl, K., Smilde, A. K. & Kiers, H. A. Cross-validation of component models: A critical look at current methods. Analytical and Bioanalytical Chemistry (2008) doi:[10.1007/s00216-007-1790-1](https://doi.org/10.1007/s00216-007-1790-1).

61. Bickel, S. & Scheffer, T. Multi-view clustering. in Proceedings - fourth ieee international conference on data mining, icdm 2004 (2004). doi:[10.1109/ICDM.2004.10095](https://doi.org/10.1109/ICDM.2004.10095).

62. Wang, Y., Wu, L., Lin, X. & Gao, J. Multiview Spectral Clustering via Structured Low-Rank Matrix Factorization. IEEE Transactions on Neural Networks and Learning Systems (2018) doi:[10.1109/TNNLS.2017.2777489](https://doi.org/10.1109/TNNLS.2017.2777489).

63. Eddelbuettel, D. & Balamuta, J. J. Extending R with C++: A Brief Introduction to Rcpp. American Statistician (2018) doi:[10.1080/00031305.2017.1375990](https://doi.org/10.1080/00031305.2017.1375990).

64. Avants, B., Johnson, H. & Tustison, N. Neuroinformatics and the the insight toolkit. Frontiers in Neuroinformatics **9**, (2015).
65. Avants, B. et al. A reproducible evaluation of ANTs similarity metric performance in brain image registration. NeuroImage **54**, (2011).
66. Muschelli, J. et al. Neuroconductor: An R platform for medical imaging analysis. Biostatistics (2019) doi:[10.1093/biostatistics/kxx068](https://doi.org/10.1093/biostatistics/kxx068).
67. Zou, H., Hastie, T. & Tibshirani, R. Sparse principal component analysis. Journal of Computational and Graphical Statistics (2006) doi:[10.1198/106186006X113430](https://doi.org/10.1198/106186006X113430).
68. Shen, H. & Huang, J. Z. Sparse principal component analysis via regularized low rank matrix approximation. Journal of Multivariate Analysis (2008) doi:[10.1016/j.jmva.2007.06.007](https://doi.org/10.1016/j.jmva.2007.06.007).
69. Jolliffe, I. T., Trendafilov, N. T. & Uddin, M. A Modified Principal Component Technique Based on the LASSO. Journal of Computational and Graphical Statistics (2003) doi:[10.1198/1061860032148](https://doi.org/10.1198/1061860032148).
70. Lin, C. J. Projected gradient methods for nonnegative matrix factorization. Neural Computation (2007) doi:[10.1162/neco.2007.19.10.2756](https://doi.org/10.1162/neco.2007.19.10.2756).
71. Jain, P., Netrapalli, P. & Sanghavi, S. Low-rank matrix completion using alternating minimization. in Proceedings of the annual acm symposium on theory of computing (2013). doi:[10.1145/2488608.2488693](https://doi.org/10.1145/2488608.2488693).
72. Blumensath, T. & Davies, M. E. Iterative hard thresholding for compressed sensing. Applied and Computational Harmonic Analysis (2009) doi:[10.1016/j.acha.2009.04.002](https://doi.org/10.1016/j.acha.2009.04.002).
73. Pustina, D., Avants, B., Faseyitan, O. K., Medaglia, J. D. & Coslett, H. B. Improved accuracy of lesion to symptom mapping with multivariate sparse canonical correlations. Neuropsychologia **115**, 154–166 (2018).
74. Hanafi, M. PLS Path modelling: Computation of latent variables with the estimation mode B. Computational Statistics (2007) doi:[10.1007/s00180-007-0042-3](https://doi.org/10.1007/s00180-007-0042-3).
75. Tenenhaus, A., Philippe, C. & Frouin, V. Computational Statistics and Data Analysis Kernel Generalized Canonical Correlation Analysis. Computational Statistics and Data Analysis (2015) doi:[10.1016/j.csda.2015.04.004](https://doi.org/10.1016/j.csda.2015.04.004).
76. Malkov, Y. A. & Yashunin, D. A. Efficient and Robust Approximate Nearest Neighbor Search Using Hierarchical Navigable Small World Graphs. IEEE Transactions on Pattern Analysis and Machine Intelligence (2020) doi:[10.1109/TPAMI.2018.2889473](https://doi.org/10.1109/TPAMI.2018.2889473).
77. Hill, W. G. & Robertson, A. Linkage disequilibrium in finite populations. Theoretical and Applied Genetics (1968) doi:[10.1007/BF01245622](https://doi.org/10.1007/BF01245622).
78. Bahmani, S. & Raj, B. A unifying analysis of projected gradient descent for lp- constrained least squares. Applied and Computational Harmonic Analysis (2013) doi:[10.1016/j.acha.2012.07.004](https://doi.org/10.1016/j.acha.2012.07.004).

79. Martí, R., Resende, M. G. & Ribeiro, C. C. Multi-start methods for combinatorial optimization. European Journal of Operational Research (2013) doi:[10.1016/j.ejor.2012.10.012](https://doi.org/10.1016/j.ejor.2012.10.012).
80. Song, G., Avants, B. & Gee, J. Multi-start method with prior learning for image registration. in Proceedings of the iee international conference on computer vision (2007). doi:[10.1109/ICCV.2007.4409159](https://doi.org/10.1109/ICCV.2007.4409159).